Correction of SLM Distortion Phase and Generation of Vortex Beams

Shi Kuo and Zhang Gongjian
Chitose Institute of Science and Technology, Chitose 066-8655, Japan,
Fax: 81-123-27-6118, e-mail: m2190070@photon.chitose.ac.jp

In recent years, with the continuous development of laser applications, scientists have developed a strong interest in the research of new laser beam theories and experiments. Among them, the dark hollow beam with zero central intensity has attracted more and more attention due to its extensive application in atomic optics, quantum optics, binary optics, manipulation of microscopic particles, and laser microscopy. These beams generally have a special helical phase wavefront structure. In this study, SLM is used to generate vortex light of any order and any topological charge, and many problems faced in the application of SLM are discussed. Since the phase modulation of SLM is undistorted under ideal conditions, however, in its manufacturing process, its optical modulation part will inevitably produce minor distortion and defects. In fact, these distortions will bring large errors to the experimental results. In order to eliminate this kind of error, this paper proposes a method to correct SLM error. We firstly accurately measured its distorted phase, and then corrected it. And taking the occurrence of vortex beams as examples, the correction effect is verified.
Key words: vortex beam, computer generated hologram, spatial light modulator.

1. INTRODUCTION

There are a series of problems in obtaining vortex beams using traditional optical systems, such as device complexity and adjustment difficulties [1]. However, it is easy to convert the light beam by using computer - generated holography in spatial light modulator (SLM). A SLM is an object that imposes some form of spatially varying modulation on a beam of light. SLM can modulate the physical parameters such as the phase, polarization plane, amplitude, intensity and transmission direction of the light beam according to the input information. Only by changing the input information, the parameters of the SLM can be controlled by the computer. Using SLM instead of traditional optical system, we can easily solve the above problems. Using SLM instead of traditional optical system, we can easily solve the above problems. In 2007, Yoshiyuki Ohtake[2] et al. used SLM to generate LG (Laguerre Gaussian) beams with radial index p and angular index l of order 5 and order 1, respectively, and realized programmable phase modulation. A computer was used to simulate the light intensity distribution of the LG beams during transmission. In this paper, three kinds of vortex beams, Bessel beams, LG beams and HyG (hypergeometric) beams are generated by reflective SLM. The interference method was used to verify their vorticity and topological charge. The HyG beam is theoretically simulated by numerical calculation, and the simulated value is compared with the experimental value, and the error is analyzed. Due to the manufacturing process, the SLM surface will have minor defects, so the use of SLM will cause the modulation phase distortion. In this paper we proposed a method to measure and correct the distortion phase of SLM.

2. THEORETICAL DESCRIPTION

2.1 Bessel beams

The field distribution of the BG beam propagating in the z direction can be expressed as [3]:

$$BG_l(r,\phi,z)=\exp\left(-i\frac{k_t^2}{2k}\frac{z}{\mu}\right)\frac{\exp(ikz)}{\mu}\times\exp\left(-\frac{r^2}{\mu\omega_0^2}\right)J_l\left(\frac{k_t r}{\mu}\right)\exp(in\phi) \quad (1)$$

where k is the wave vector, J_l is the first kind *l* order Bessel function, exp(inφ) represents the spiral phase structure, n is the topological charge, $k_t=k\sin\theta$ is the radial component of the wave vector, and ksin(θ) corresponds to the spatial carrier frequency. Furthermore, $\mu=\mu(z)=(1+iz/z_R)$, where $z_R=k\omega_0^2/2$ shows the Rayleigh distance.

2.2 HyG beams

In cylindrical coordinates, the field distribution of the hypergeometric beams at the incident surface (z =

0) is [4]

$$E(r,\varphi,z=0)=\frac{E_0}{2\pi}\left(\frac{r}{\omega}\right)^m \exp\left(-\frac{r^2}{2\sigma^2}+i\gamma \ln\frac{r}{\omega}+in\varphi\right) \quad (2)$$

2.3 Laguerre Gaussian beams

The Laguerre Gaussian (LG) beams propagating in the direction (z) can be mathematically described by the following equation [5]:

$$LG_p^l(r,\varphi,z)=\frac{(-1)^p}{\omega}\sqrt{\frac{2}{\pi}\frac{p\ !}{(p+|l|)!}}\times\left(\frac{\sqrt{2}r}{\omega}\right)^{|l|}L_p^{|l|}\left(\frac{2r^2}{\omega^2}\right)\exp\left(\frac{-r^2}{\omega^2}\right)\times\exp\left(-in\varphi-\frac{ir^2z}{\omega^2 z_R}\right)\times\exp\left(i(2p+|l|+1)\tan^{-1}\left(\frac{z}{z_R}\right)\right) \quad (3)$$

where p is the radial index and l is the angular index, ω is the beam waist radius, $L_p^l(x)$ is the Laguerre polynomial, z_R is the Rayleigh length, and $\tan^{-1}(z / z_R)$ is the Gouy phase.

The transmission function of CGH is defined in reference [6]. Through the vortex beam $U_1(r,\phi,z)=A_1\exp[i(kz-ar-p\phi)]$ and plane wave $U_2(r,\varphi,z)=A_2\exp[i(kz+k_x r\cos\varphi)]$ interference obtain. In this equation, $k_x=k\sin\varepsilon$ is the wave vector component along the x-axis, ε corresponds to the angle between the wave vector and the x-axis. The following expression shows the transmission function of CGH:

$$T(r,\phi)=|U_1+U_2|^2=\sum_{m=-\infty}^{+\infty}t_m\exp(-im(ar-p\phi+\beta r\cos\phi)) \quad (4)$$

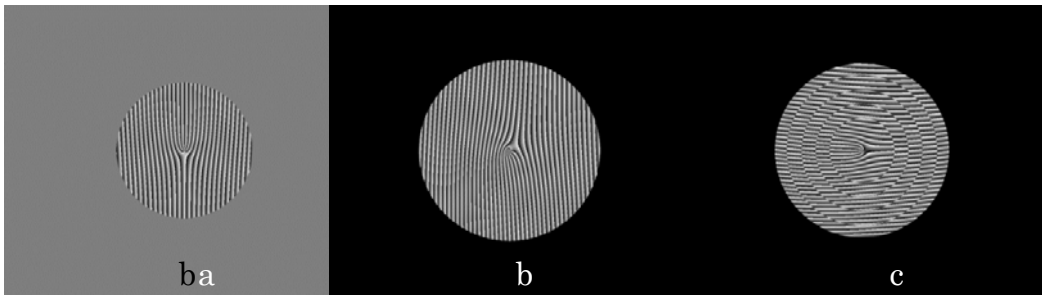

Fig. 1. Several type of holographic masks. (a) CGH with topological charges p=5 and axicon base angles γ=0°, (b) CGH of Hypergeometric Beams, and (c) CGH of Lagurrer-Gaussian Beams

3. EXPERIMENTAL

3.1 Scheme and experimental setup for creating and verifying vortex beam

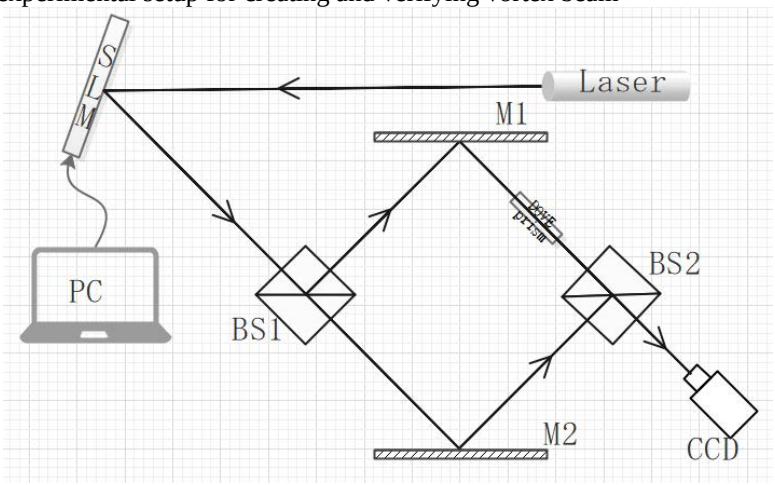

Fig. 2. Vortex beam generation and verification experimental device, M1 and M2 are plane mirrors, BS1 and BS2 are beam splitters.

The experimental setup is shown in Figure 2. It consists of a computer holographic display system and a verification system. Computer holographic display system consists of He-Ne laser with wavelength λ =

632.8 nm, reflective liquid crystal SLM and PC. The PC is used to upload the MSK into the SLM, and the laser light is reflected by the light modulation unit of the SLM to complete modulation.

The interferometer consists of plane mirrors M1 and M2, beam splitters BS1 and BS2, DOVE prism, and the CCD is used to record the interference signal. When two vortex beams whose topological charges are n (n is an integer greater than 1) and opposite directions interfere, 2n interference bright spots will appear. M1, M2, BS1, BS2, and DOVE prism are used to form a Mach-Zehnder interferometer system to check the obtained beam. The DOVE prism can change the vortex direction.

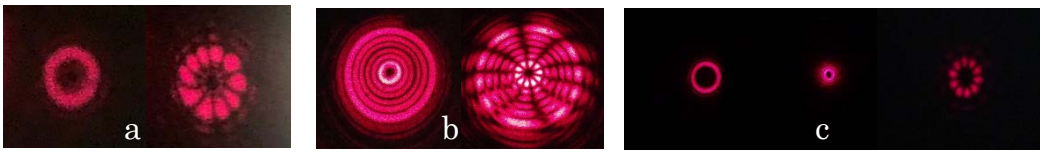

Fig. 3. Diffraction beam intensity diagram and its interference diagram with topological charge n=5 (a) Bessel beams intensity diagram and its interference diagram, (b) LG beams intensity diagram and its interference diagram, and (c) HyG beams intensity diagram and its positive first-order diffraction interference diagram.

Experimental results are shown in figure 3. The image on the left of each figure (a, b and c) is the intensity distribution of the vortex beam diffracted by SLM, while the image on the right is the interference pattern obtained by the interferometer interference of the diffracted beam. In the interferograms (on the right of each figure), the number of spots of interference is 10, which proves that three kinds of vortex beams with topological charge n=5 are successfully obtained in this experiment.

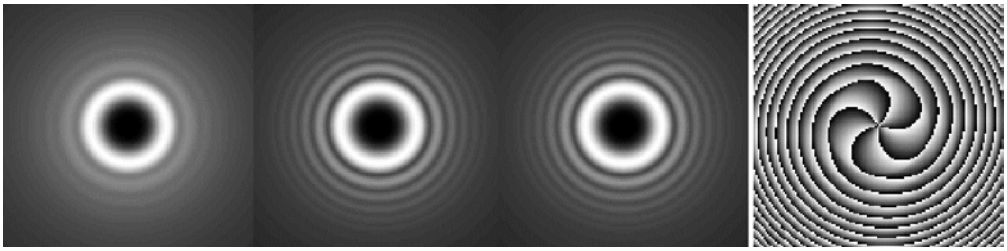

Fig. 4. Simulation values of diffraction integral light intensity and phase distribution. The calculation parameters from left to right are a = 5, 50, 5000 respectively.

3.2 Comparison of simulation and experiment

By substituting Eq. (2) into the generalized Huygens-Fresnel diffraction integral, we get

$$E(\rho,\theta,z)=\frac{(-1)^{n}i^{1-n}kE_0}{2\pi z}\exp\left(-\frac{ikD\rho^2}{2z}\right)\exp(in\theta)\times\int_0^{\infty}A_p(r)\left(\frac{r}{\omega}\right)^{m+i\gamma}\exp\left[-\left(\frac{1}{2\sigma^2}+i\frac{k}{2z}\right)r^2\right]J_n\left(\frac{k\rho r}{z}\right)rdr \quad (5)$$

where k is the wave number, J_n is the Bessel function of the first kind, and A_p (r) is

$$A_p(r)=\begin{cases}1, & r\le a\\ 0, & r>a\end{cases} \quad (6)$$

where a is the diaphragm radius. Considering that the hard-edged circular aperture function can be extended to the sum of a set of complex Gaussian functions, we can get the following expression

$$A_p(r)=\sum_{h=1}^{N}A_h\exp\left(-\frac{B_h}{a^2}r^2\right) \quad (7)$$

where A_h and B_h are extended complex Gaussian coefficients, in this paper, the expansion coefficients in reference [7] are selected for calculation. Substituting Eq. (7) into Eq. (5), and using the integral formula

$$\int_0^{\infty}x^{a-1}\exp(-px^2)J_v(cx)dx=c^{v}p^{-(v+a)/2}2^{-v-1}\Gamma\left(\frac{v+a}{2}\right)\ {}_1F_1\left(\frac{v+a}{2},v+1,-\frac{c^2}{4p}\right), \quad (8)$$

rearranging the above, we have

$$E(\rho,\theta,z)=\frac{(-1)^{n}i^{1-n}kE_0}{2\pi z}\exp\left(-\frac{ik\rho^2}{2z}\right)\exp(in\phi)\times\sum_{h=1}^{N}A_h\left(\frac{1}{\omega}\right)^{m+i\gamma}\left(\frac{k\rho}{z}\right)^{n}\left(\frac{B_h}{a^2}+\frac{1}{2\sigma^2}+i\frac{k}{2z}\right)^{-(m+n+i\gamma+2)/2}\times\Gamma\left(\frac{m+n+i\gamma+2}{2}\right)\Gamma^{-1}(n+1)\times{}_1F_1\left(\frac{m+n+i\gamma+2}{2},n1,-\frac{(k\rho/z)^2}{4(B_h/a^2+1/2\sigma^2+ik/2z)}\right) \quad (9)$$

where ${}_1F_1(a, b, x)$ is a hypergeometric function and $\Gamma(x)$ is a gamma function. Eq. (9) is the diffraction field distribution of CGH with diaphragm constraint (aperture radius A). Its light intensity can be calculated using the formula $I = |E(\rho, \theta, z)|^2$.

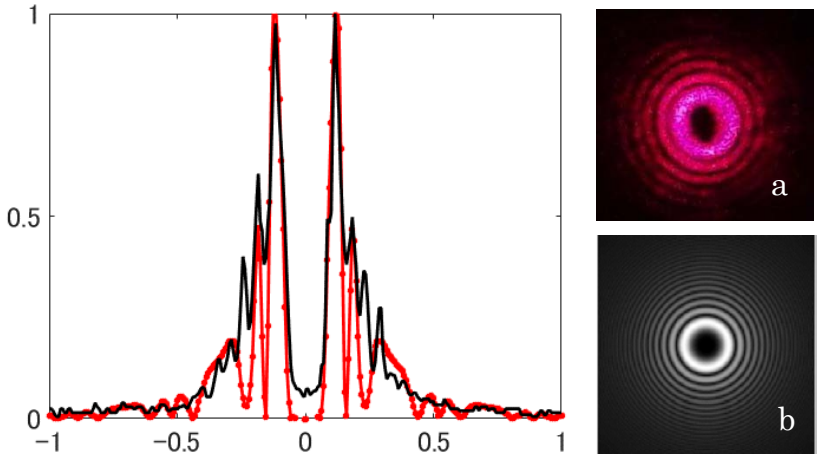

Fig. 5. HyG beams diffraction intensity profile experiment(a) and simulation value(b) fitting

Table 1. Analysis of fitting errors

SNR	Err2	RNew1	RNew2	MAE	RMSE	X_{corr_coef}
2.1092	1.4873	0.5917	0.6122	1.4873	0.6399	0.9221

We use the experimental value I_{the} and the simulation value I_{cal} to define several quantities [10] that can reflect the fitting accuracy, they are the overall signal-to-noise ratio of the beam intensity profile distribution

$$SNR = \sum_n I_{the}(n) / \sum_n |I_{the}(n) - I_{cal}(n)|, \tag{10}$$

two new quantities defined by the concept of deviation

$$R1 = 1 - \sqrt{\sum_n (I_{the}(n) - I_{cal}(n))^2 / \sum_n I_{the}^2(n)} \tag{11}$$

$$R2 = 1 - \sqrt{\frac{\sum_n (I_{the}(n) - I_{cal}(n))^2}{\sum_n I_{cal}^2(n)}}, \tag{12}$$

mean absolute error

$$MAE = \sum_n |I_{the}(n) - I_{cal}(n)| / N, \tag{13}$$

and root mean square error

$$RMSE = \sqrt{\sum_n (I_{the}(n) - I_{cal}(n))^2} / N. \tag{14}$$

4. MEASUREMENT AND CORRECTION OF DISTORTION PHASE OF SLM

The basic principle of phase-shifting interferometry [9] is: Phase shifting devices (half wave plate, quarter wave plate, polarizing plate or diffraction grating, etc.) are added to the reference light path of the optical system to orderly change the phase difference between the reference light wave and the object light wave.

The obtained interferograms are recorded using detectors such as CCD. Since the intensity distribution of the interferogram is the cosine function of the phase change caused by the surface shape of the object to be measured, by analyzing and demodulating the phase-shift interferograms, the wrapping phase information of the object to be measured can be solved, and then continuous phase information can be obtained through the phase-unwrapping algorithm, so as to reconstruct the surface contour or three-dimensional morphology of the object to be measured.

The phase shift method is divided into 4-step phase shift method and multi-step phase shift method. The calculation formula of the 4-step phase shift method is

$$\varphi = \arctan\left\{\frac{\sqrt{[(I_2 - I_3) + (I_1 - I_4)] * [3 * (I_2 - I_3) + (I_1 - I_4)]}}{(I_2 - I_3) - (I_1 - I_4)}\right\} \tag{15}$$

where I_1 to I_4 are 4 interferograms with constant phase shift difference. However, the easiest method to implement is the two-step phase shift method, which means that the phase information can be obtained by collecting two interferograms with different phase differences.

The intensity of interference fringes can be expressed by $I(x,y) = a(x,y) + b(x,y) * cos(\varphi(x,y) + \delta)$, where $a(x,y)$ is the background term of the interferogram, and $b(x,y)$ is the modulation term of the interferogram, $\varphi(x,y)$ is the phase of the sample surface, δ is the phase of the reference light path. The background item a(x,y) of the interferogram is generally a low-frequency dc signal, which can be filtered by Gaussian high-pass filter. After processing, the interference fringe becomes $\tilde{I}(x,y) = b(x,y) * cos(\varphi(x,y) + \delta)$.

For any two interferograms,

$$\tilde{I}_1 = b(x,y) * cos(\varphi + \delta_1) \quad (16)$$

$$\tilde{I}_2 = b(x,y) * cos(\varphi + \delta_2) \quad (17)$$

let's take $\delta_1 = 0$, $\delta_2 = \delta$, for convenience, and we get

$$\tilde{I}_1 = b(x,y) * cos(\varphi) \quad (18)$$

$$\tilde{I}_2 = b(x,y) * cos(\varphi + \delta) \quad (19)$$

rearranging the above, we have

$$\varphi = arctan\left(\frac{\tilde{I}_1\ cos(\delta) - \tilde{I}_2}{\tilde{I}_1\ sin(\delta)}\right), \quad (20)$$

(24)

The phase difference can be obtained as followings [11]

$$\delta = \arccos\left(\frac{\langle \tilde{I}_1, \tilde{I}_2 \rangle}{\langle \tilde{I}_1, \tilde{I}_1 \rangle}\right) \quad (25)$$

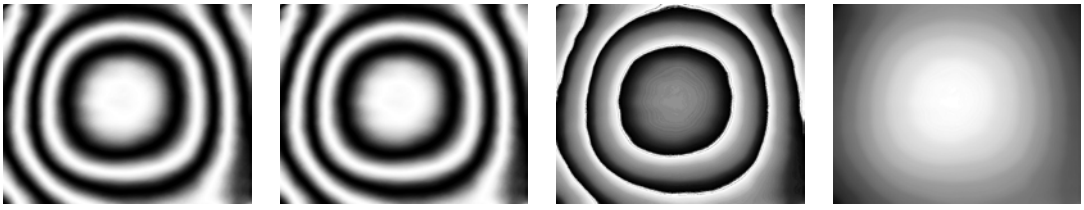

a b c d

Fig. 6. Phase shifted interferogram and distortion phase distribution.

The figure a and b in Fig. 6 are the interference patterns processed by using a Gaussian high-pass filter, these two interferograms were taken at different amount of phase shift. The figure (c) is the wrapped SLM surface distortion phase obtained from interferograms, and (d) is unwrapped phase. Fig. 7 are photographs of diffracted vortex beam. The left one is the diffracted beam without correction of distortion phase, and right is that with correction of distortion phase.

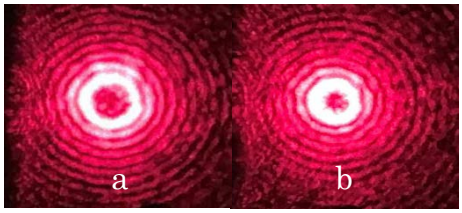

Fig. 7. Diffraction light intensity distribution (a)before phase correction (b)after distortion phase distribution

CONCLUSIONS

In summary, with the development of fine processing technology, it becomes possible to perform high-precision modulation of the light wavefront through equipment such as liquid crystal SLM. We have carried out theoretical analysis and experimental research, and successfully generated Bessel beams, LG beams and HyG beams using computer holographic display technology. And the theoretical simulation and experimental value fitting of HyG beam are carried out. At the same time, a fast and relatively accurate

method for correcting and measuring the distorted phase of SLM surface is also proposed.

References

[1] Coullet, P., L. Gil, and F. Rocca. "Optical vortices." Optics Communications, **73**, 5, 403-408 (1989).
[2] Ohtake, Yoshiyuki, et al. "Universal generation of higher-order multiringed Laguerre-Gaussian beams by using a spatial light modulator." Optics letters, **32**, 11, 1411-1413(2007).
[3] Karahroudi, Mahdi Khodadadi, et al. "Generation of perfect optical vortices using a Bessel–Gaussian beam diffracted by curved fork grating." Applied optics, **56**, 21, 5817-5823(2017).
[4] Kotlyar, V. V., et al. "Hypergeometric modes." Optics Letters, **32**, 7, 742-744(2007).
[5] Guo S. F., Liu K., Sun H. X., et al. “Generation of Higher-order Laguerre-Gaussian Beams by Liquid Crystal Spatial Light Modulators,” Journal of Quantumn Optics, **21**, 1, 86-92(2015). (in chinese)
[6] Topuzoski, Suzana. "Generation of optical vortices with curved fork-shaped holograms." Optical and Quantum Electronics, **48**, 2, 138(2016).
[7] Wen, J. J., and M. A. Breazeale. "A diffraction beam field expressed as the superposition of Gaussian beams." The Journal of the Acoustical Society of America, **83**, 5, 1752-1756(1988).
[8] A. Erdelyi, W Magnus, F. Oberhettinger. “Tables of integral transforms [M]”, McGraw-Hill, (1953).
[9] Malacara Z., Servin M., “Interferogram analysis for optical testing [M]”, CRC press, (2005).
[10] Gongjian, Zhang, Zhang Man, and Zhao Yang. "Wave front control with SLM and simulation of light wave diffraction." Optics express **26**, 26, 33543-33564 (2018).
[11] Niu, Wenhu, et al. "Phase shifts extraction algorithm based on Gram–Schmidt orthonormalization of two vectors." Optical and Quantum Electronics **47**, 8, 2803-2810 (2015).